Local loss coefficients inside air cavity of ventilated pitched roofs

Gullbrekken, L., Uvsløkk, S., Geving, S., & Kvande, T.

Citation for the published version (APA 6th)
Gullbrekken, L., Uvsløkk, S., Geving, S., & Kvande, T. (2018). Local loss coefficients inside air cavity of ventilated pitched roofs. *Journal of Building Physics*, *42*(3), 197–219.

Local loss coefficients inside air cavity of ventilated pitched roofs

Lars Gullbrekken[1], Sivert Uvsløkk[2], Stig Geving[1] and Tore Kvande[1]

Abstract
Pitched roofs with a ventilated air cavity to avoid snow melt and ensure dry conditions beneath the roofing is a widely used construction in northern parts of Europe and America. The purpose of this study has been to determine pressure losses at the inlet (eaves) and inside the air cavity consisting of friction losses and passing of tile battens. These results are necessary to increase the accuracy of ventilation calculations of pitched roofs. Laboratory measurements, numerical analysis as well as calculations by use of empirical expressions have been used in the study.
A large difference in the local loss coefficients depending on the edge design and height of the tile batten was found. The local loss coefficients of the round-edged tile battens was approximately 40 % lower than the local loss coefficients of the sharp-edged tile battens. Further, the local loss factor increased by increasing height of the tile batten. The numerical analysis was found to reliably reproduce the results from the measurements.

Keywords
Laboratory measurements, local loss coefficients, COMSOL, roofing ventilation, air cavity, tile batten

Introduction

Ventilated pitched roofs are currently a widely used construction for residential and non-residential buildings in northern parts of Europe and America. The air cavity beneath the roofing is ventilated to ensure dry conditions for the roof construction and keep the roofing temperature low enough to avoid snow melt. The construction is of special interest regarding the dry-out capacity in roofs with load-bearing systems of wood. When built in line with the guidelines given by Roels and Langmans (2016), Uvsløkk (1996), and Edvardsen and Ramstad (2014), ventilated pitched wooden roofs can be considered a robust roof design. However, there are well-known degradation issues related to snow melt and mould growth. Tobiasson et al. (1994) studied icing problems in northern America,

[1]Department of Civil and Environmental Engineering, Norwegian University of Science and Technology (NTNU), Trondheim, Norway

[2]Department of Materials and Structures, SINTEF Building and Infrastructure, SINTEF, Trondheim, Norway.

Corresponding author:
Lars Gullbrekken, Norwegian University of Science and Technology (NTNU), Høgskoleringen 7 A 7046, Trondheim, Norway.
Email: lars.gullbrekken@sintef.no

and they reported that the icing problems of several buildings in northern New York were reduced by increasing the ventilation of the attics so that the temperature inside the attics was below -1 °C when the external temperature was -5.5 °C. Measurements performed in Canada by Walker and Forest (1995) showed that attic ventilation was mainly driven by wind and that the ventilation increased by increasing wind speeds. The problem with snow melt on roofs is reduced in modern well-insulated roofs with well-ventilated roofing (Geving, 2011).

In the Nordic countries, the moisture conditions inside cold ventilated attics have been studied. In Sweden, Samuelson (1998) found that a reduction in the ventilation of the attics caused a drier climate inside the attic. However, the calculations assumed a totally airtight ceiling structure beneath the attic. In Norway, Blom (2001) conducted field measurements and calculations of ventilation of pitched wooden roofs with cold attics. Blom found that a 48 mm high air cavity was appropriate in pitched, ventilated single-family houses. Blom also pointed out that a key factor in moisture-safe constructions is to ensure continuous thermal insulation and avoid air leakages through the insulation.

The current Norwegian guidelines for pitched roofs as given by Edvardsen and Ramstad (2014) are too simplified. In particular, there are no common guidelines for roof constructions with low angles, complicated roof design, roof spans longer than 7.5 m and roofs with building-integrated photovoltaics (BIPV).

The driving forces given by wind and temperature differences (natural convection) together with the calculated pressure losses in the air cavity below the roofing define the ventilation rate of pitched wooden roofs. Important input parameters required to calculate the wind-driven ventilation of pitched roofs include wind speed together with the difference in wind pressure coefficient, c_p, at the inlet and the outlet of the ventilation cavity (see Figure 1). Pressure losses in the roof system including where the air passes (hereafter called "passing") the inlet and outlet, passing of tile battens and friction losses are calculated based on the input data. The accuracy of these calculations obviously depends on the accuracy of the local loss coefficients for the passing of the inlet, tile battens and outlet.

The purpose of this study has been to determine pressure losses at the inlet (eaves) and inside the air cavity consisting of friction losses and passing of tile battens.

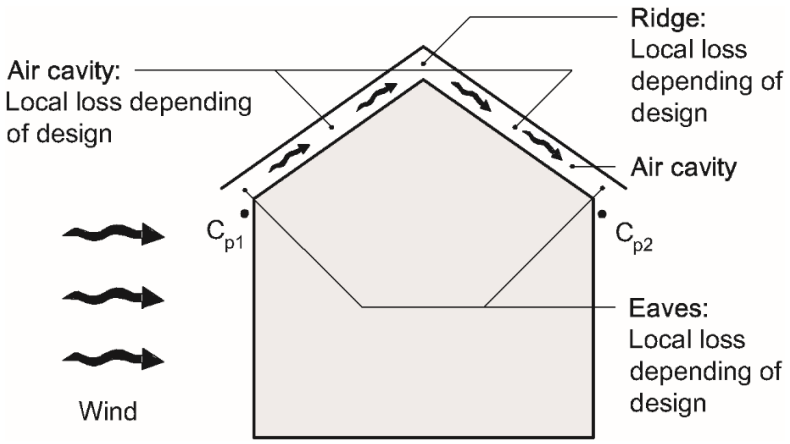

Figure 1. Important input parameters to calculate the wind-driven ventilation of pitched wooden roofs include wind speed together with the difference in wind pressure

coefficient, c_p, at the inlet and outlet of the ventilation cavity as well as local losses inside the air cavity.

Theoretical framework

The air flow through the air cavity system $\dot{V}$ (m³/h) can be expressed by eq. (1), where the air flow is proportional to the driving forces of roof ventilation, Δp (Pa), given by the driving forces of wind and buoyancy. The air flow is inversely proportional to the sum of pressure losses through the air cavity system, R (Pa), in the following treated as friction loss and local losses.

$$\dot{V} = \sum \Delta p \cdot \frac{1}{\sum R} \qquad (1)$$

Pressure losses and velocity profiles of pipes and air channels have previously been studied both theoretically and experimentally. The extensive work has led to empirical expressions for accurately calculating the pressure loss given well-defined flow situations, see e.g. (Hansen et al., 2013).

The Reynolds number indicates whether a flow is laminar or turbulent: small Reynolds numbers give laminar flow while large numbers give turbulent flow. The critical Reynolds number gives the value of the Reynolds number for the transition from laminar to turbulent flow. The size of the critical Reynolds number is dependent on the flow characteristics, sharp edges and change in velocity. For most flows, the critical Reynolds number is 2300 (Hansen et al., 2013).

$$\mathrm{Re} = \frac{u \cdot D_h}{\nu} \qquad (2)$$

Re is the Reynolds number (-), u is the average velocity (m/s), D_h is the hydraulic diameter (m) of the flow channel and ν is the kinematic viscosity (m²/s).

Friction loss

The pressure loss gradient (Pa/m), p_Δ inside a channel is dependent on the dynamic pressure p_d (Pa), the hydraulic diameter D_h (m) and the friction number λ (-).

$$p_\Delta = \lambda \frac{p_d}{D_h} \qquad (3)$$

The dynamic pressure, p_d (Pa), is given by:

$$p_d = \frac{1}{2} \cdot \rho \cdot u_m{}^2 \qquad (4)$$

Where ρ is the density of the air (kg/m³) and u_m is the average air velocity (m/s).

The hydraulic diameter, D_h (m), is given by:

$$D_h = \frac{2 \cdot a \cdot b}{a + b} \qquad (5)$$

Where a and b are the side lengths of the rectangular air channel (m).

For laminar flow, the friction number λ (-) is inversely proportional with the Reynolds number, Re.

$$\lambda = \frac{64}{\mathrm{Re}} \qquad (6)$$

Local losses

Pressure losses in components like valves and bends are called local losses. Flow characteristics can be studied by applying established equations from fluid mechanics. Local pressure loss is given by the local loss coefficient, see eq. (7) and (8). For ξ=0 the local loss is zero and for ξ=1 the local loss is equal to the dynamic pressure. At steady state, the driving forces are balanced by the pressure loss from friction and the pressure loss of the different minor losses along the flow path.

$$\Delta P = \xi \cdot \frac{\rho \cdot u_m{}^2}{2} \qquad (7)$$

$$\xi = \frac{2 \cdot \Delta P}{\rho \cdot u_m{}^2} \qquad (8)$$

Where ΔP is the pressure loss (Pa), ξ is the minor loss coefficient (-), ρ is the density of the air (kg/m³), u_m is the average velocity (m/s). u_m is given by the airflow Q(m³/s) divided by the area of the smallest cross-section of the flow path A(m²).

Narrowing of the flow channel

The pressure loss in a narrowing cross-sectional flow area is caused by a contraction of the flow after the narrowing, given by the contraction factor α (see equation 10 (Hansen et al., 2013) and Figure 2).

$$\xi_1 = \left(\frac{1}{\alpha} - 1\right)^2 \qquad (9)$$

$$\alpha = \frac{\mathrm{A}_0}{\mathrm{A}_2} \qquad (10)$$

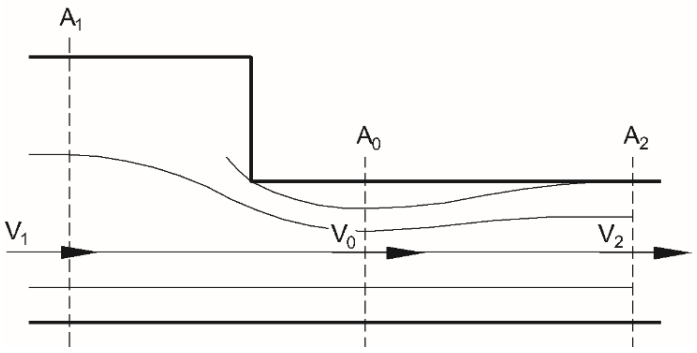

Figure 2. Pressure loss when there is a sharp decrease in the cross-sectional flow area.

Contraction of the flow channel

Pressure loss when there is a sharp increase in the cross-sectional flow area can be calculated using eq. 11, giving the local pressure loss as a function of the cross-sectional area before and after the component (Hansen et al., 2013), see Figure 3.

$$\xi_2 = \left(1 - \frac{A_1}{A_2}\right) \qquad (11)$$

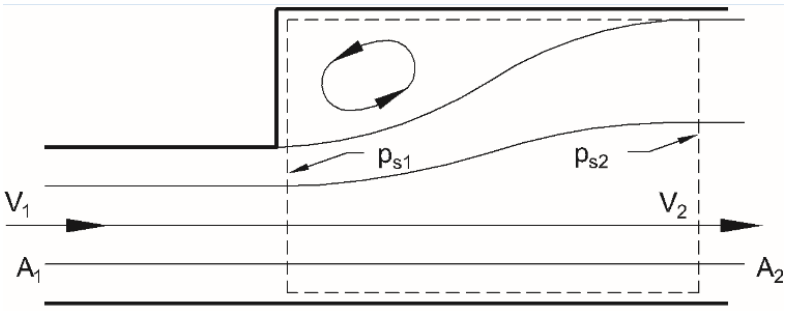

Figure 3. Pressure loss when there is a sharp increase in the cross-sectional flow area.

The total local loss given by the local loss by contraction of the channel, ξ_1 (-), and local loss by narrowing of the channels, ξ_2 (-), can be calculated using eq. (12).

$$\xi = \xi_1 + \xi_2 \qquad (12)$$

Previous research

In a laboratory study, Thiis et al. (2007) studied different roof eave designs and their inlet geometry in order to specify the ability to reduce snow penetration into the roof. The geometry and design of the ventilation openings was found to be the most important factor in reducing snow penetration. An inlet position close to the wall was found to give approximately 5 times more snow concentration of the air entering the roof cavity compared to a position close to the end of the eave.

Idelchik (1994) contains a systematization and classification of data of hydraulic resistances from a large number of experimental studies carried out and published at different times in different countries.

Kronvall (1980) conducted measurements of airflow in building components and showed how the concept of fluid mechanics could be applied to airflow in building components. He also studied pressure losses at the entrance and bends in duct flows.

Later, Hofseth (2004) studied airflows in ventilated roof structures. As part of his work, he performed laboratory measurements of local losses of building components located inside the air cavity of the roof. He found that the local loss coefficient was dependent on the mass flow.

Falk and Sandin (2013) also performed laboratory measurements to estimate loss factors of metal battens inside ventilated wall cavities. They found that several of the loss factors were dependent on the air velocity.

Methods

The method includes both a laboratory investigation on a large-scale test model of a pitched wooden roof and numerical analysis using COMSOL software.

Laboratory test model

A large-scale test model of the ventilation air gap of a pitched roof was built in the SINTEF and NTNU laboratory in Trondheim, Norway. The model consisted of an aluminium profile with a length of 3550 mm and an internal width of 552 mm (see Figure 4). As shown in Figure 4, the width of the box corresponds to the air gap between two counter battens with a width of 48 mm and a centre-to-centre distance of 600 mm, which is a typical situation in a ventilated wooden roof. As seen in Figure 5 and Figure 6, the total length of the roof test model was 3550 mm and included a total of 11 tile battens with a centre-to-centre distance of 350 mm. Nine air pressure nipples were positioned in the top of the box, as seen in Figure 6.

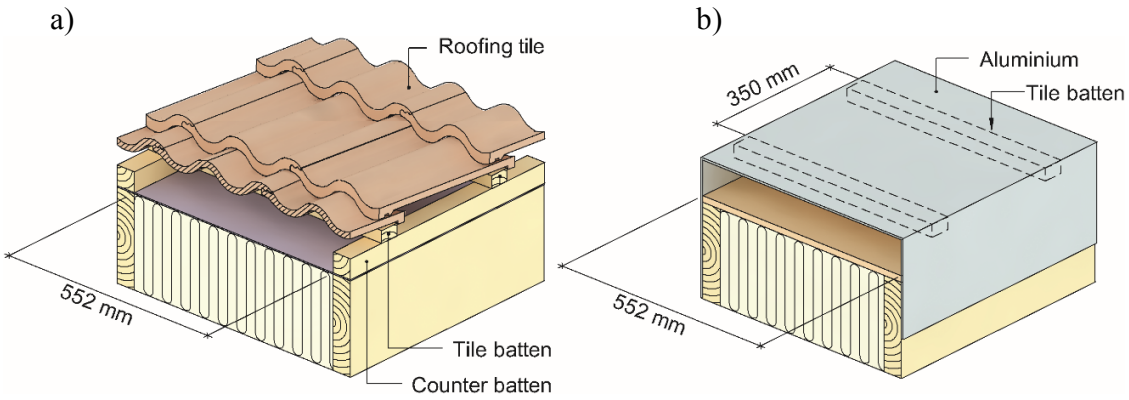

Figure 4. a) Cross-section of a typical roof construction with roofing tiles. b) A cross-section of the test model consisting of an aluminium box corresponding to the air gap between two counter battens with a width of 48 mm and a centre-to-centre distance of 600 mm. The center to center distance of the tile battens are 350 mm

The airflow through the roof structure is measured by a laminar flow meter which is attached to a fan that sucks air through the ventilation gap system. In order to measure the pressure differences, four pressure transmitters (Furness Controls FCO 352 Model 1) were used. The pressure difference was recorded with a data logger (Delphin Technology Expert Key 100C) with a logger interval of 1 Hz (see Figure 5). Each measuring step lasted approximately 120 s. The accuracy and measuring range of the applied instruments are given in Table 1.

Table 1: Accuracy and measuring range of applied sensors

Sensor	Manufacturer	Type	Accuracy	Range
Thermocouple		Type T	±0.10 °C	-20–+60 °C
Pressure transmitter	Furness Control	FCO 352 Model 1	±0.25 % of reading	0–+50 Pa
Folding rule			±0.5 mm	0–2000 mm

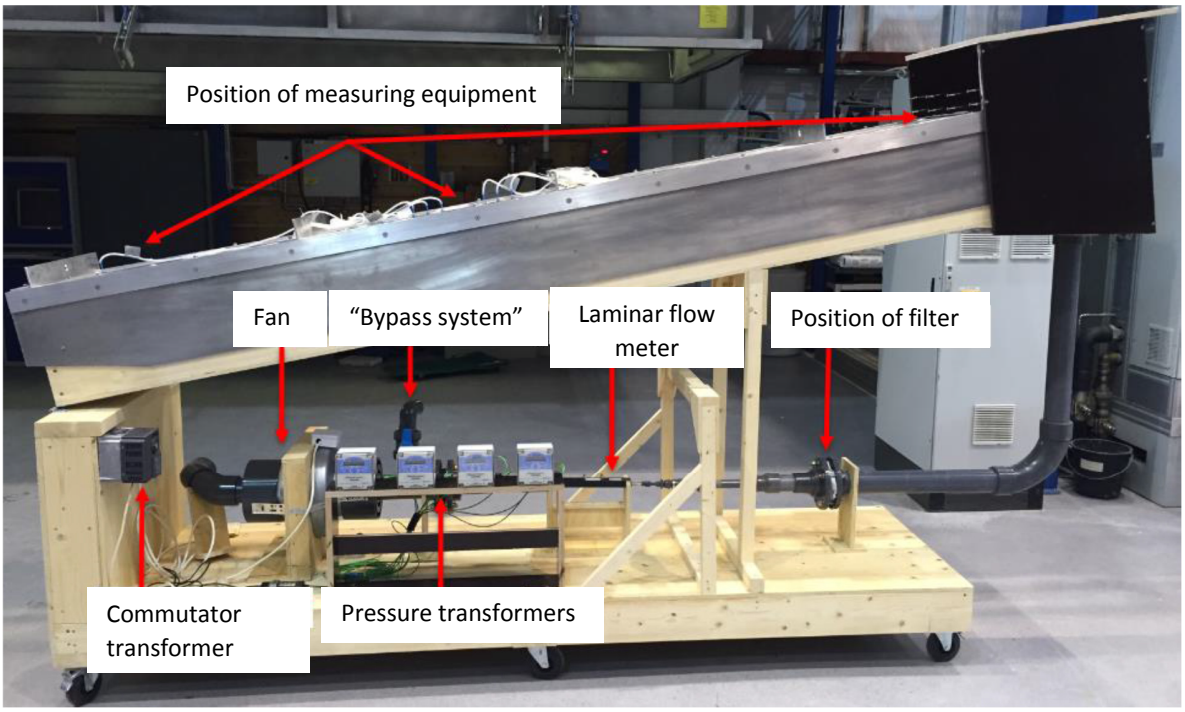

Figure 5. A large-scale test model of a pitched roof.

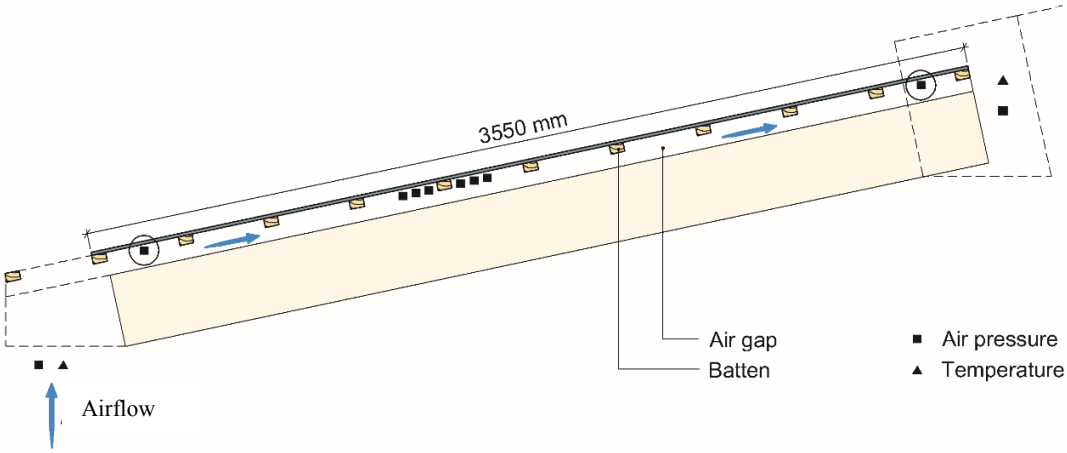

Figure 6. Cross-section of the test model, with ten air pressure monitor positions. The figures for the air pressure difference of the two points with circles, divided by the number of tile batten passings, which is nine, are used as input in eq. (8).

Test procedure

The range of the air gap, height of the air cavity and center-to-center distance of the tile batten was determined by an investigation into the Norwegian building traditions described in Edvardsen and Ramstad (2014). In order to obtain as realistic measurements as possible the results a field investigation of air velocity inside the air cavity of a roof was studied (Gullbrekken 2017). He reported air velocity inside the air cavity for different seasons/periods as a function of wind speed at 10 m above ground level. The reported air velocity inside the air cavity was 0-1.2 m/s. The results were in line with a previous and corresponding investigation reported by Blom (1990). In addition, an important aspect was to choose air velocities that produced measurable static air pressure difference when passing battens. Simple calculations by use of eq. (9-12) was performed in order to predict the pressure difference.

The test procedure was performed by installation of tile battens in the measuring rig, as showed in Figure 6. Then, the correct height of the air cavity beneath the tile batten was adjusted (23, 36 or 48 mm). The air flow was adjusted in order to fit the dynamic pressures of 0.05, 0.10, 0.20, 0.40 Pa. This implies an increasing airflow by increasing height of the air cavity beneath the tile battens. A specific air flow was held constant in 30 s and the data was logged with 1Hz logging interval. Then, a new air flow was set and held constant in 30 s and so on.

Table 2 Test parameters, the chosen parameters and the reference to the chosen parameters.

Test parameters	Chosen parameters	Reference
Height of the air gap	23, 36, 48 (mm)	Edvardsen and Ramstad (2014)
Height of tile battens	30, 36, 48 (mm)	Edvardsen and Ramstad (2014)
Center to center distance tile battens	350 (mm)	Edvardsen and Ramstad (2014)
Air velocity below tile battens (corresponding dynamic pressure) (Pa)	0.20, 0.40, 0.60, 0.80 (m/s)	Gullbrekken (2017), Blom (1990)

Different design of the eave

In order to study the local pressure loss coefficient at the inlet of the ventilation cavity, we studied two different eave design solutions.

Classic design

A classic air inlet design in Norway has one or several air gaps in the horizontal part of the eave construction (see Figure 7 a)). The laboratory investigation included measurements of local loss coefficients given one air gap with a width of 50 mm with and without installation of a fly net with an opening area of 67 % covering the gap opening.

Modern design

Stricter requirements regarding airtightness of buildings necessitates a continuous wind barrier between wall and roof, as seen in Figure 7 b). In this case, the air inlet of the roof ventilation system is a 25 mm wide air gap behind the gutter. The laboratory investigation included measurements of local loss coefficients with and without a fly net covering the gap opening. The fly net had an opening area of 67 %.

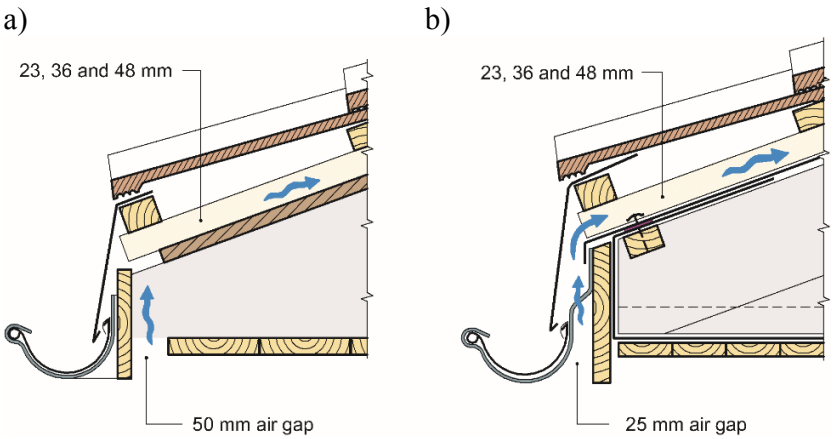

Figure 7. The two different eaves designs. a) A classic solution with one air gap behind the gutter board. b) a newer design with the air gap located between the gutter and the gutter board.

Airtightness of the laboratory test model

Initially, the airtightness of the test model was measured. The joints between the aluminium box and the rest of the test rig were sealed using tape. In addition, the inlet of the test rig was sealed. The measurements showed that the airflow through the sealed test model was less than 0.6 % of the smallest tested airflow. By adding the rafter detail, the airflow through the sealed test model increased to 2.5 % compared to the smallest tested airflow.

Uncertainty assessment of the laboratory measurements

The root-mean square (RMS) method was used to derive the total uncertainty propagation of the measured local loss coefficients, $\frac{\Delta^p \xi}{\xi}$, see eq. (16) and (17).

$$\xi = \frac{2 \cdot \Delta P}{\rho \cdot u_m{}^2} \tag{12}$$

$$\Delta P = P_1 - P_2 \tag{13}$$

$$\rho_{cavity} = \frac{\theta_{293.15K} \cdot \rho_{293.15K}}{\theta_{cavity}} = \frac{a}{T} \tag{14}$$

$$u_m^2 = \left(\frac{q}{A} \right)^2 \tag{15}$$

$$\xi = \frac{2 \cdot \Delta P \cdot T \cdot A^2 \cdot 60000^2}{a \cdot q^2} \tag{16}$$

$$\frac{\Delta^p \xi}{\xi} = \sqrt{\left[\frac{\Delta^p (\Delta P)}{(\Delta P)} \right]^2 + \left[\frac{\Delta^p T}{T} \right]^2 + \left[\frac{\Delta^p A}{A} \right]^2 + \left[\frac{\Delta^p q}{q} \right]^2} \tag{17}$$

Where P_1 (Pa) and P_2 (Pa) is the static air pressure at the particular measuring positions. u_m (m/s) is the average air velocity in the smallest cross section of the particular cross section. ρ is the density of the air (kg/m³), θ is the temperature (K), q is the air flow (m³/h) and A is the area of the smallest cross section of the air cavity of the particular cross section. Where, $\frac{\Delta^p (\Delta P)}{(\Delta P)}$ is the uncertainty in the measured air pressure differences, $\frac{\Delta^p T}{T}$ is the uncertainty in the air temperature measurements, $\frac{\Delta^p A}{A}$ is the uncertainty in the cross sectional area of the air cavity and the tile batten, $\frac{\Delta^p q}{q}$ is the uncertainty of the measured air flow through the air cavity.

No correlation between the various terms of the equation was found. The accuracy and measuring range of the applied instruments are given by Table 1.

Numerical analysis

Laboratory measurements are expensive and takes a lot of time. Compared to laboratory measurements numerical analysis implies a large reduction of time and the possibility to investigate a larger span of design variation. Therefore, it is valuable to compare measurements with simulations of the current study. In the current study, numerical analysis includes simulation of airflow inside the air cavity between the underlayer roofing and the roofing material. Conservation of mass, momentum and energy is based on the assumption of a flowing media with constant properties. In the laminar regime, the flow of the media can be predicted by solving the steady-state Navier–Stokes equations given in eq. (18).

$$\rho \left[\frac{dv}{dt} + u + \nabla u \right] = \nabla \cdot \sigma + f \tag{18}$$

Where ρ denotes the density of the fluid (kg/m³), u is the velocity (m/s), $\nabla \cdot \sigma$ denotes shear stress and f being all other forces.
This can be rewritten assuming a Newtonian fluid:

$$\rho\left[\frac{dv}{dt} + u + \nabla u\right] = -\nabla p + \mu\nabla^2 u + f \qquad (19)$$

Where p is the pressure (Pa) and μ (Pa s) is the dynamic viscosity.

$$\nabla p = \mu\nabla^2 u + f - \rho\left[\frac{dv}{dt} + u + \nabla u\right] \qquad (20)$$

COMSOL Multiphysics software has been used for mesh generation and to solve the system of partial differential equations.

The COMSOL Multiphysics software include eight built-in turbulence models. They differ how they model the flow close to the wall, number of additional variables solved for and what theses variables represent. Among them are the Low Re k-ε-model and Low Re k-ω-model. The term "Low Reynolds number does not refer to the flow on a global scale, but in the region close to the wall where viscous effects dominate. A low Reynolds number model therefore more correctly reproduces the behaviour of different flows at small distances from the wall. The Low Re k-ε-model solves for two variables: k, the turbulence kinetic energy; and ε, the rate of dissipation of turbulence energy. A wall function is used in the model. In that way the flow close to the surfaces is not simulated. The Low Re k-ω-model is a model similar to the k-ε-model, but it solves for ω, the specific rate of dissipation of kinetic energy. The model is more nonlinear and therefore somewhat more difficult to converge. The model is useful in many cases when the k-ε-model is not accurate. In this work we have used both models. The k-ε-model that is more easily converging is used to find a prelimenary solution. Based on the solution the k-ω-model is used to increase the accuracy of the solution. A coarse grid is used in the solver in order to lower the period to perform the simulations, however even so one calculation including four air velocities took several hours!

Calculation of the minor losses was performed according to eq. (8). The static pressures of the simulations was read from the simulation model according to the laboratory measurements. The position of the static pressure of the model is indicated by red dots in Figure 8.

Simulation model

In order to simplify the model and thereby reduce the time needed for calculations, the model only included passing of one tile batten (see Figure 8). The simulation model has been used to calculate the loss in absolute pressure at different dynamic pressures inside the air channel and thereby calculate the local singular loss coefficients according to eq. (8). A parameter study including different dynamic pressures, dimensions of the tile batten and height of the air channel below the tile batten was conducted.

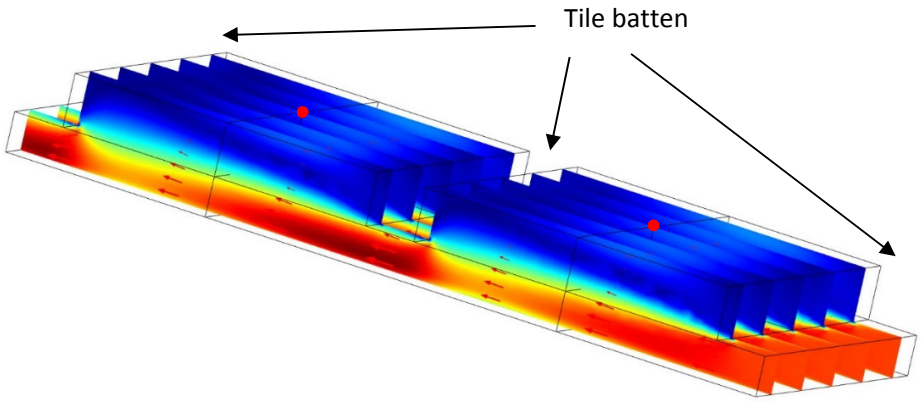

Figure 8. Five cross sections of the air velocity distribution inside the air cavity given by the COMSOL software. Higher air velocities are indicated in red color. Red dots indicate the position of the static pressure measurements used in the calculations of the minor losses

Results

Friction loss

Calculated and measured friction coefficients of the air cavity as a function of the Reynolds number are shown in Figure 9. The theoretical friction coefficient is calculated according to eq. (6) assuming that airflow inside the air channel is laminar.

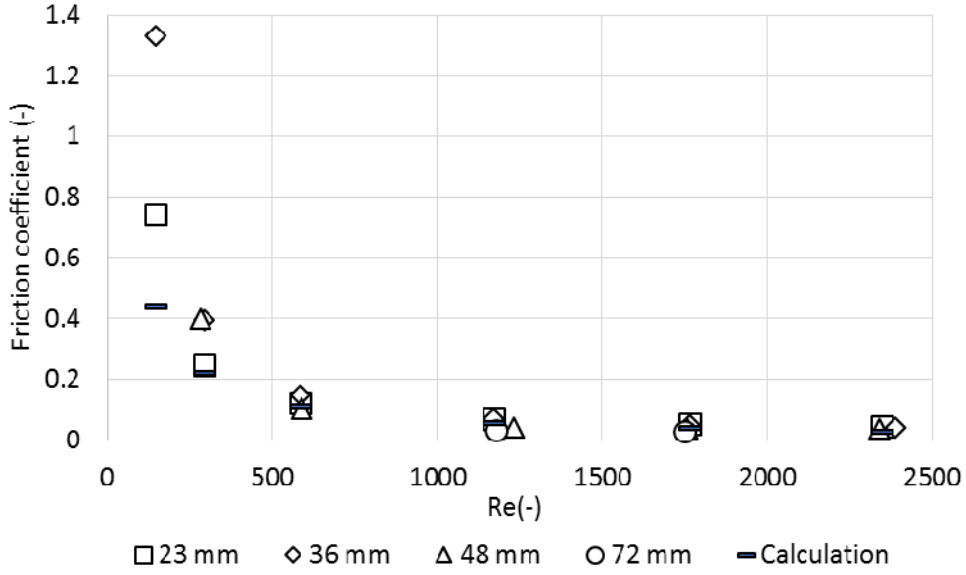

Figure 9. Calculated and measured friction coefficients in the air channel at different Reynolds numbers and counter batten thickness.

Sharp-edged and round-edged tile battens

The local loss coefficients for 36 mm sharp-edged and 36 mm round-edged tile battens for 23 mm and 48 mm air gaps are shown in Figure 10 along with theoretical values as given in the “Danvak" handbook by (Hansen et al., 2013).

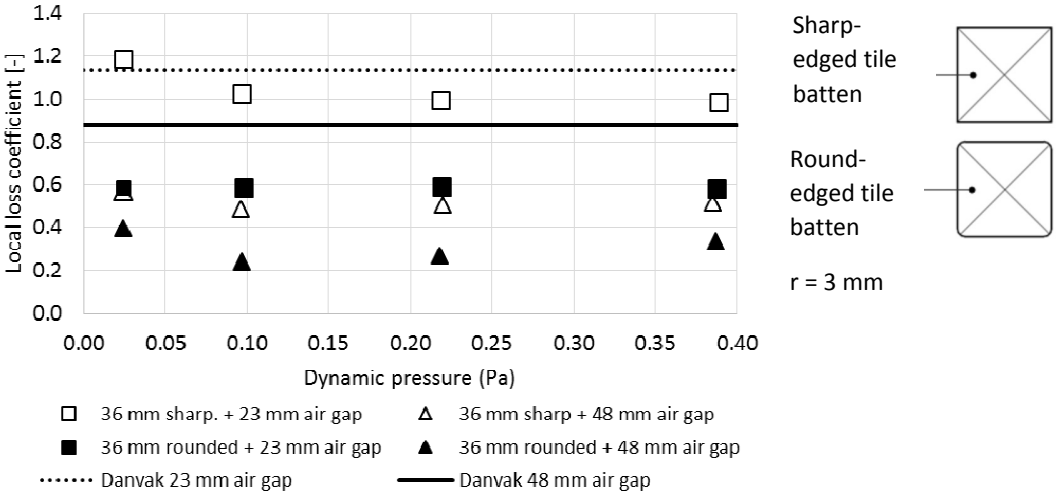

Figure 10. Local loss coefficient for sharp-edged and rounded battens with different air gaps and dynamic air pressure of the airflow passing the tile batten. “Danvak” means values calculated from Hansen et al. (2013).

Different dimensions of tile and counter battens

Figure 11 shows local loss coefficients for tile battens that are 30 mm, 36 mm and 48 mm high and air cavity heights of 23 mm, 36 mm and 48 mm below the tile batten as a function of the dynamic pressure given by eq. (4). The width of the tile batten is kept constant at 48 mm. The open symbols represent the results of the measurements, the filled symbols represent results from the COMSOL calculations, and the straight lines represent calculated values according to equations 10, 11 and 12 given in the “Danvak" handbook (Hansen et al., 2013).

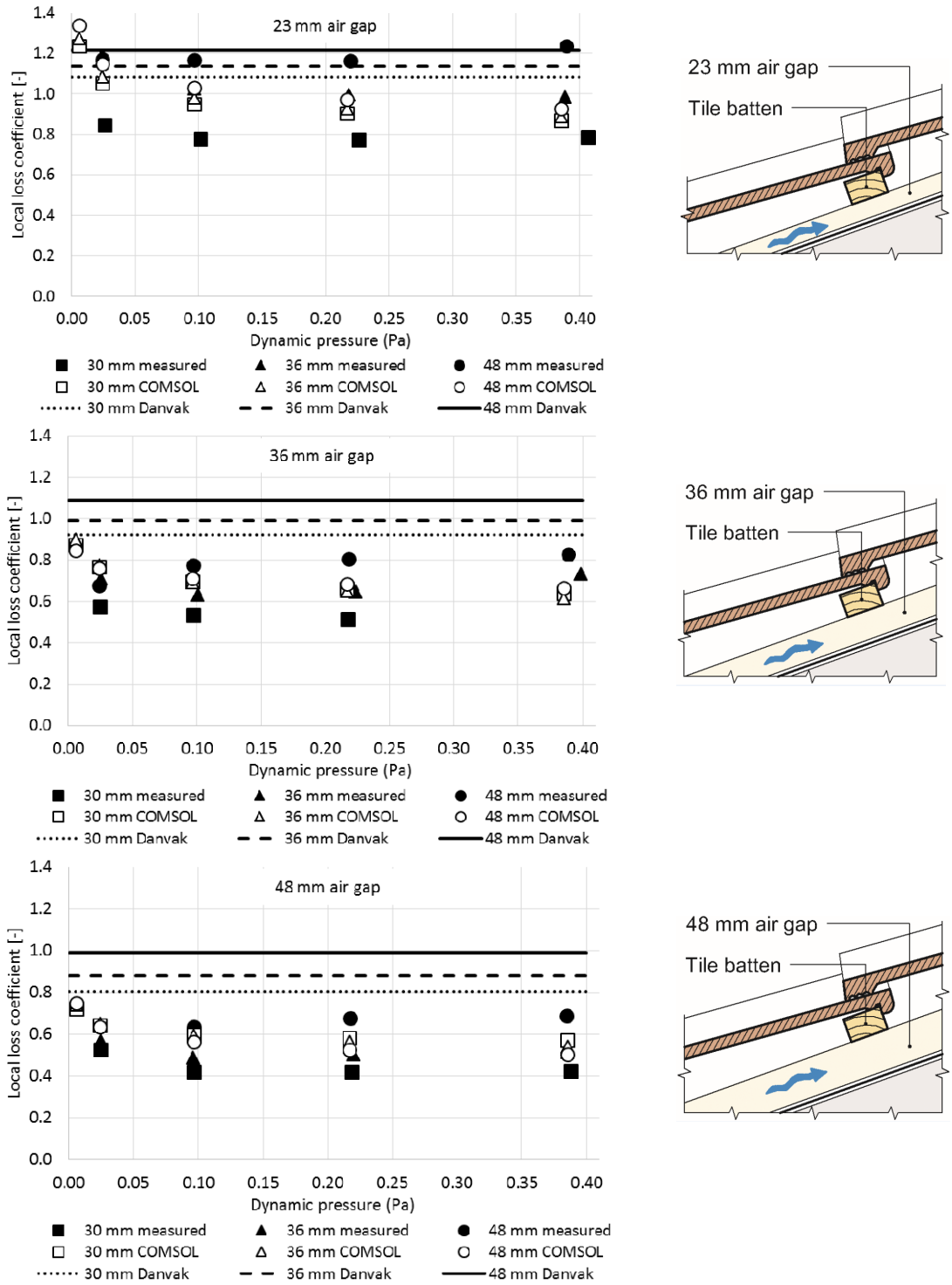

Figure 11. Local loss coefficient as a function of dynamic pressure for tile battens that are 30, 36 and 48 mm high. The filled symbols represent the results of the measurements, the open symbols represent results from the COMSOL calculations, and the straight lines represent theoretical values according to equations 10, 11 and 12 given in “Danvak" handbook (Hansen et al., 2013).

In order to simplify the measuring results, eq. (21) and (22) describes the local loss coefficient by passing of one sharp edged batten. β in eq. (22) is given by A_1 and A_2 in Figure 2. Equation 21 is derived by regression analysis and least square method. With a starting point in eq. (9) the formulae was adjusted in order to obtain as small deviation between the measuring results and the equation as possible. Figure 12 shows the calculated results from eq. (21) compared to the measured results for the 36 mm air gap.

$$\xi = -\left(\frac{1}{\beta} - 1.375\right)^3 \qquad (21)$$

$$\beta = \frac{A_1}{A_2} \qquad (22)$$

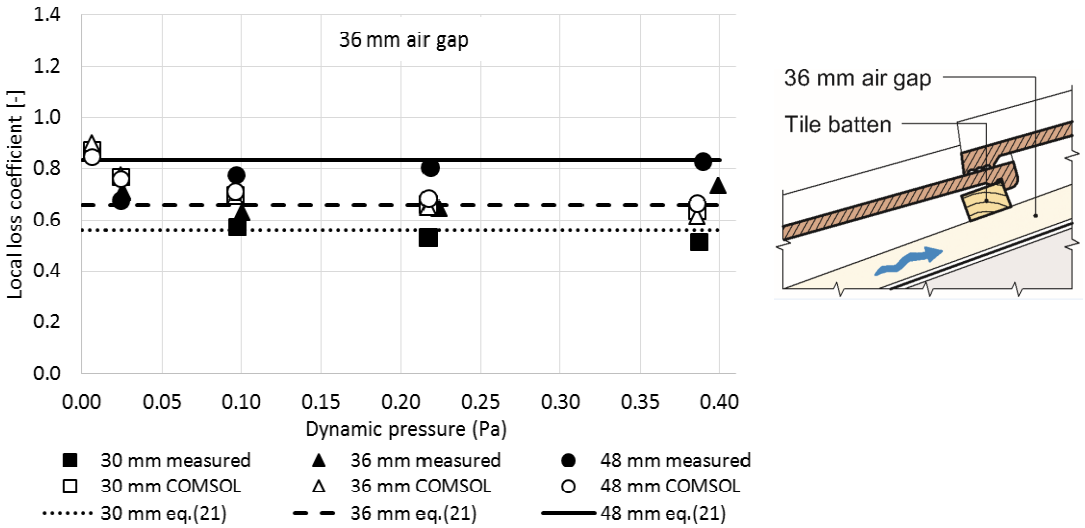

Figure 12. The filled symbols represent the results of the measurements, the open symbols represent results from the COMSOL calculations, and the straight lines represent values according to eq. (21).

Table 3 shows the average measured local loss coefficient by assuming a constant relation between the local loss coefficient and the dynamic pressure. In the table, the measured values are compared to the calculated values according to Hansen et al. (2013 and to results from eq. (21) which is a improved solution based on the laboratory measurements.

Table 3 Average measured and calculated local loss coefficients.

Air gap (mm)	Tile batten (mm)	Average measured local loss coefficient, ξ	Standard deviation, measured values	Calculated local loss coefficient, ξ eq. (9-12)	% difference compared to measurements	Calculated local loss coefficient ξ eq. (21)	% difference compared to measurements
	30	0.78	0.006	1.08	28 %	0.82	5 %
23	36	1	0.023	1.14	12 %	0.94	-6 %
	48	1.19	0.04	1.22	2 %	1.14	-4 %
	30	0.54	0.032	0.92	41 %	0.56	4 %
36	36	0.67	0.055	0.99	32 %	0.66	-2 %
	48	0.8	0.025	1.09	27 %	0.83	4 %
	30	0.42	0.003	0.81	48 %	0.43	2 %
48	36	0.5	0.013	0.88	43 %	0.51	2 %
	48	0.67	0.028	0.99	32 %	0.66	-2 %

Uncertainty of the tile batten measurements

Each calculated local loss coefficients of the tile batten consist of three measurements; Two friction loss measurements (the friction loss between and below the tile batten) and a measurement of pressure loss including local losses by tile battens and friction. The uncertainty has only been calculated for part of the measurements as given by Table 4.

Table 4 Average measured local loss coefficient and the calculated local loss and the percentage difference between the two values.

	23 mm cavity		48 mm cavity	
Dynamic pressure	0.1 Pa	0.4 Pa	0.1 Pa	0.4 Pa
Tile batten height (mm)	$\Delta\xi$ (%)	$\Delta\xi$ (%)	$\Delta\xi$ (%)	$\Delta\xi$ (%)
30	10.3	10.7	5.0	4.4
36	9.9	10.1	4.4	4.4
48	9.1	9.1	4.3	4.3

Air intake at eaves

Classic design

Figure 13 shows the local loss coefficient of the air intake design as a function of the dynamic pressure in the air cavity beneath the tile battens. The pressure is measured at the black dots in Figure 13. The figure shows results from one air gap of 50 mm with and without a fly net. The different series in the diagram are related to measurements performed with 23, 36 and 48 mm air gaps beneath the tile battens. The height of the tile batten is kept constant at 36 mm.

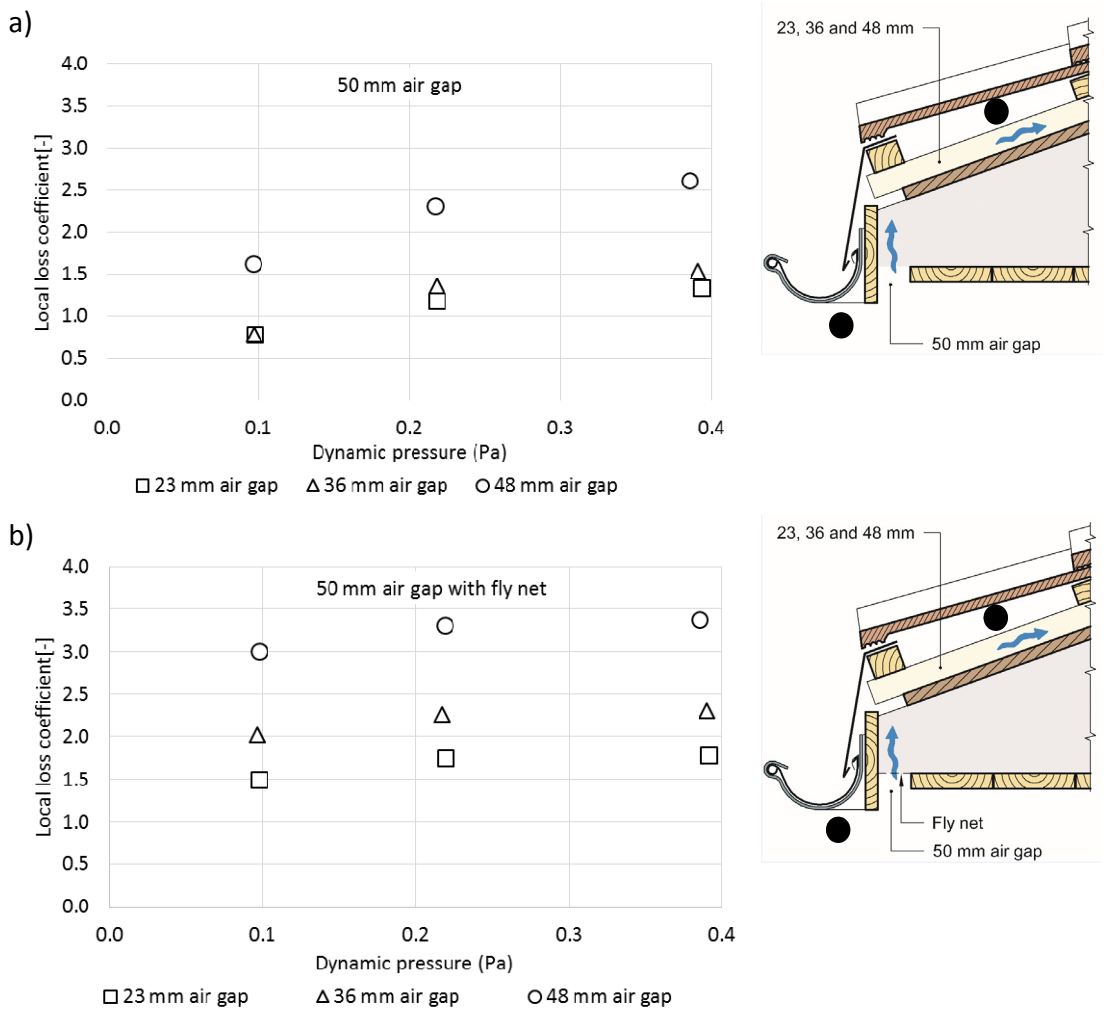

Figure 13. Measuring results of local loss coefficient for the classic eaves design as a function of dynamic pressure calculated for the air cavity beneath the tile batten. The pressure is measured at the black dots.

Modern design

Figure 14 gives the minor loss coefficient of the detail as a function of the dynamic pressure in the airflow beneath the tile batten. The pressure is measured at the black dots in Figure 14. The local loss coefficients in Figure 14 are corrected by subtracting the pressure loss caused by the passing of one tile batten. The figure shows results from one air gap of 25 mm with and without a fly net. The different series in the diagram are related to measurements performed with 23, 36 and 48 mm air gaps beneath the tile battens. The height of the tile batten is kept constant at 36 mm.

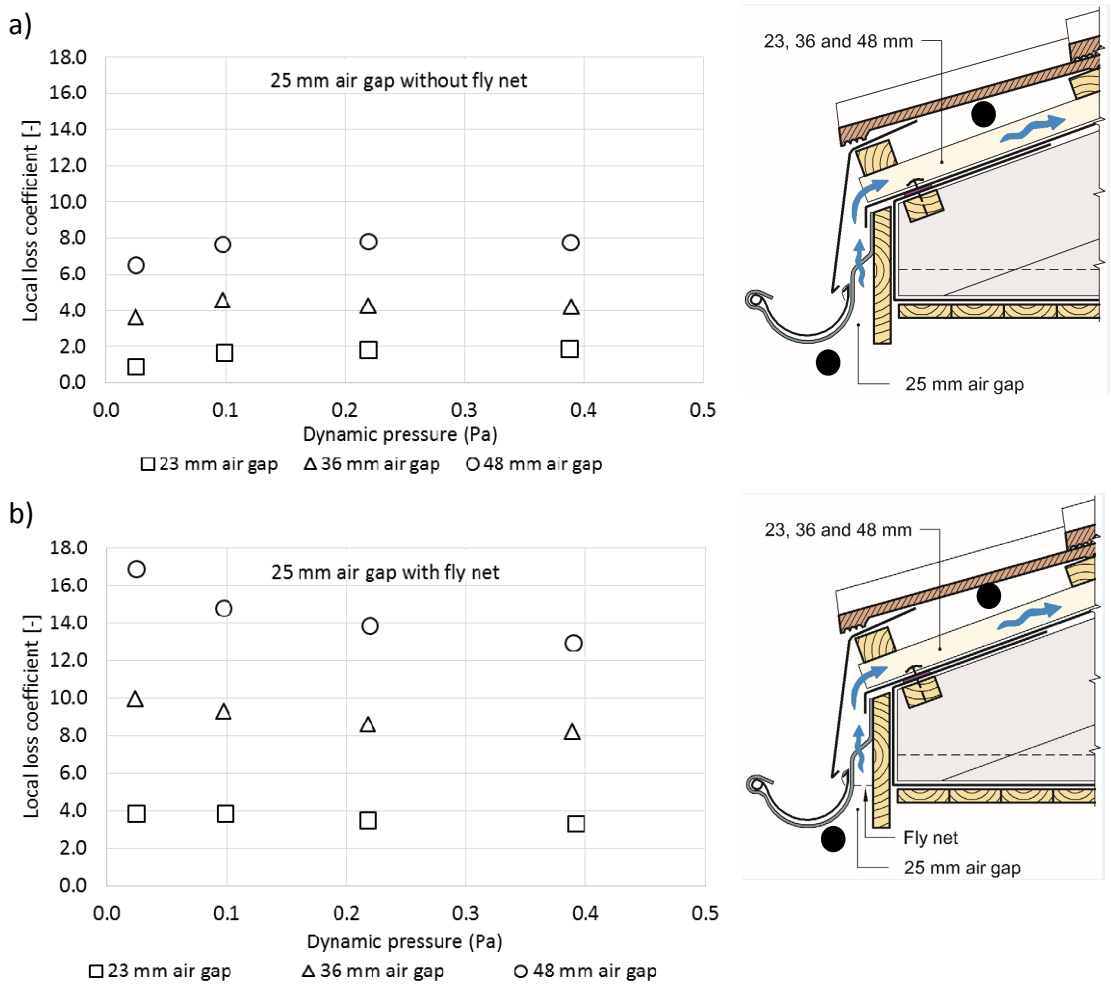

Figure 14. Measuring results of local loss coefficient for the modern eaves design as a function of dynamic pressure calculated for the air cavity beneath the tile batten. The pressure is measured at the black dots.

Discussion

The results show a good correspondence between the measured friction coefficient and the calculated friction coefficient. The calculated Reynolds numbers of Figure 8 indicate laminar flow. Therefore, the friction coefficient is inversely proportional to the Reynolds number.

Laboratory measuring model compared to tile roofing

The design of the laboratory measurements can be directly compared to using membranes on wooden boards for roofing. Use of metal sheeting or tiles implies an air gap between the roofing and the tile batten. An air gap above the tile batten roofing will affect the flow pattern of the airflow. It is likely that the increased cross-sectional area available for airflow

will reduce the local loss coefficient. Consequently, the measured local loss coefficients of this study are conservative.

The effect of roof slope is not covered by this study. However, the slope will affect the local loss at the eaves because the deflecting of the air flow entering the air cavity is dependent of the roof slope.

The height of the tile batten

In general, both the measurements and COMSOL-simulations showed smaller local loss coefficients compared to the calculations using the "Danvak" handbook (eq. (9-12)). Eq. (9-12) are general values given a narrowing and contraction of the air flow. In this case there is a small distance between the narrowing and contracting of the air flow possibly not causing completely laminar and undisturbed air flow when the air passes the contraction. Eq. (21) is an improvement of the eq. (9-12) and is specific for the passing of sharp edged tile battens. According to Kronvall (1980), a short distance between two obstacles in an airflow will cause a reduction of the total local loss coefficient given by the two obstacles. The calculations, simulations and the measurements all showed increasing local loss coefficients in line with increasing height of the tile batten. By assuming a constant relation between the local loss coefficient and the dynamic pressure, a deviation between the measured and calculated values of 3–80 % was found. The maximum deviation between the average calculated local loss coefficient and average measured local loss coefficient was 48 %. The equivalent number for eq. (21) was 9 %. Hence, a sufficient correspondence between the calculated local loss coefficients for a batten passing given by eq. (21) and the measurements was found. The smallest deviation was found for the smallest air cavity and the largest height of the tile batten. The measurements of the smallest air gaps and largest tile battens suggests a maximum 4 Pa pressure drop over nine tile battens. A larger measured pressure difference reduces the errors from the resolution in the pressure transmitter and fluctuations in the surrounding air.

The measurements and simulations of different dimensions of the tile batten indicated a constant correlation between the local loss coefficient and the dynamic pressure given a larger dynamic pressure than 0.10 Pa. However, both Hofseth (2004) and Falk and Sandin (2013) found that the local loss coefficient was dependent on the air velocity and hence the dynamic pressure. The air velocity of Hofseth's results was 5–10 times larger than the air velocity of the current study. This will of course influence the flow characteristics inside the air cavity. The air velocity of Falk and Sandin (2013) was of the same magnitude as the current study. Measurements at low dynamic pressures mean that the measured pressure drop over the nine tile battens is very small, typically down to 0.1 Pa, which could imply increased measuring error, both because of the resolution of the pressure transmitter and fluctuations in the surrounding air.

However, the calculations of uncertainty do not interpret a correlation between the dynamic pressure and the magnitude of the uncertainty. On the other hand, the magnitude of uncertainty seems to increase by decreasing height of the air cavity below the tile batten. One possible explanation is that the relative measuring error of the cross-sectional areas increases by decreasing height of the air cavity. Based on this explanation and the constant relation between the uncertainty and the tile batten height it is likely that the calculation of uncertainty from the 36 mm air gap will be somewhere between the two calculated uncertainties, i.e. somewhere between 5 and 10 %.

Sharp-edged and round-edged tile batten

The measurements showed a large difference in the local loss coefficients depending on the edge design of the tile batten. The local loss coefficient of the rounded tile battens was approx. 40 % lower than the local loss coefficients of the sharp-edged tile battens. Idelchik (2005) also reported lowered local loss coefficients by use of rounded orifaces. There was a larger difference between the sharp-edged and round-edged tile batten for the 48 mm air gap compared to the 23 mm air gap. Almost all the measured values showed lower local loss coefficients compared to the calculated values according to equations 9–12. The smallest deviation was found for the 23 mm air gap and the sharp-edged tile batten.

Numerical analysis

It was found that the simplified COMSOL model shown in Figure 8 could reliably reproduce the results from the measurements. The smallest deviation between the simulations and the measurements was found for the smallest dynamic pressures. Many of the measurements include low Reynolds-numbers, and the flow is laminar, but at the highest dynamic pressures the flow are turbulent or in the transition zone. A possible solution to lower the deviation at the highest Reynolds numbers is including of a different model more adapted to high Reynolds numbers. However, a challenge is that the Reynolds numbers are different in the different cross sections along the flow possibly changing between laminar and turbulent flow. The Low Re k-ω-model was used in the COMSOL simulations because of the geometry of the simulation model and the surface-position of the static air pressure used in the calculation of the local losses. It was assumed that a more accurate calculation of the flow characteristics close to the surface was important in order to obtain a more correct static pressure at the surface.

A simplification of the model is the assumption of uniform flow at the inlet of the model, below the tile batten. A close study into the second tile batten of Figure 8 shows that the air velocity is somewhat higher in the middle of the cross section and close to the lower surface compared to the air velocity close to the tile batten, also given in Figure 2. The smallest difference between the measurements and the simulations was found for the 36 mm tile batten and the air gaps of 23, 36 and 48 mm. The simulation results indicates that the tile batten height inflates less on the local loss coefficient compared to the measurements and the calculations.

The results indicate that the COMSOL software can be used to produce local loss coefficients where measurements of local loss coefficients of sharp-edged tile battens are not available. Given a larger dynamic pressure than 0.10 Pa the COMSOL simulation indicate a constant local loss coefficient. Some of the measuring results also indicate an increasing local loss coefficient at lower dynamic pressures. This phenomena is not easy to explain. The error by simplifying and calculating with a constant local loss coefficient at these small dynamic pressures will, however, be small because of low air velocities inside the cavity which, according to eq. 7, gives small pressure losses.

Eaves design

The local loss coefficient increases by increasing height of the air gap beneath the tile batten. The explanation is the increasing airflow through the eaves construction by

increasing air gap beneath the tile batten because the dynamic pressure is calculated at the passing of the tile battens. The measurements of the classic design show a large increase in the local loss coefficient by introduction of a fly net inside the 50 mm air gap at the eaves. The option without a fly net shows an increasing local loss coefficient by increasing dynamic pressures. The measurements for the option with a fly net indicate a constant relation between the dynamic pressure and the local loss coefficient for a dynamic pressure larger than 0.2 Pa. The measurements and literature review conducted by Kronvall (1980) also indicated a constant local loss coefficient independent of the Reynolds number. The measurements include narrowing and contraction when the air enters the air space inside the eaves construction. Further, the measurements include narrowing and contraction when the air enters the air cavity below the roofing. The geometry of the eaves design makes it difficult to compare the results to calculated results from equations in the literature.

The modern eaves design of Figure 13 shows increasing local loss coefficients compared to the classic solution. This can partly be explained by the decreased gap in the air cavity compared to the classic design. The measurements include pressure loss by narrowing and friction loss in the 25 mm air cavity. Further, the measurements include a bend and narrowing and contraction by passing of the lowest tile batten of the roof. As with the classic solution, the local loss coefficient increases in line with the height of the air gap and thereby increased mass flow through the air cavity. Installation of a fly net inside the air cavity leads to approximately doubling of the local loss coefficients. The increase is larges for the smallest dynamic pressures. The dynamic pressure is still calculated in the cross section below the tile batten. Installation of fly net of course reduces the effective air flow area and thereby increases the local loss coefficient.

The local loss coefficients with the classic design correspond to the local loss coefficient given by four tile batten passings without a fly net and six tile batten passings with a fly net. The local loss coefficient given by the modern design without a fly net corresponds to approximately 16 tile batten passings. By installing a fly net, the local loss coefficient corresponds approximately to 30 tile batten passings. Thiis et al. (2007) showed that an increased local loss coefficient and thereby a reduction in the air velocity inside the air cavity was effective to reduce snow penetration into the air cavity.

Measures to increase ventilation of pitched roofs

In order to increase the ventilation of a typical roof construction, a decrease in the height of the tile batten is positive as well as an increase in the counter batten height. Use of round-edged tile battens was also found to lower the local loss coefficient, by approx. 40 %, and thereby increase the ventilation of the roof compared to a sharp-edged tile batten. To increase the ventilation of pitched wooden roofs, the results show that a classic eaves design without a fly net is the preferred eaves solution.

Conclusion

This study has found a large difference in the local loss coefficients depending on the edge design of the tile batten. The local loss coefficients of the round-edged tile battens was approximately 40 % lower than the local loss coefficients of the sharp-edged tile battens. The measurements and simulations of different dimensions of the tile batten indicated a

constant correlation between the local loss coefficient and the dynamic pressure given a larger dynamic pressure than 0.10 Pa. The COMSOL model used in the study could reliably reproduce the results from the measurements. Increased height of the counter batten as well as use of rounded tile battens was found to be effective at increasing the ventilation of pitched wooden roofs. Further, the measurements showed considerably lower local loss coefficients for the classic eaves design compared to the modern design. Installation of fly net in the ventilation gap was found to approximately double the local loss coefficient.

Acknowledgements

The authors gratefully acknowledge the financial support by the Research Council of Norway and several partners through the Centre of Research-based Innovation "Klima 2050" (www.klima2050.no).

References

Blom, P. (1990) Venting of insulated, pitched roofs (In Norwegian). Dr. thesis. Institute of Building Technology. Norwegian Technical University. Trondheim. Norway.

Blom P. (2001) Venting of Attics and Pitched, Insulated Roofs. *Journal of Building Physics* 25: 32-50.

Edvardsen K, Ramstad T. (2014) *Trehus Håndbok 5 (Wood frame houses handbook no 5)(In Norwegian).* SINTEF Building and Infrastructure. Oslo. Norway

Falk J, Sandin K. (2013) Ventilated rainscreen cladding: Measurements of cavity air velocities, estimation of air change rates and evaluation of driving forces. *Building and Environment* 59: 164-176.

Geving S. (2011) *Fuktskader Årsaker, Utbedringer og tiltak*. (*Moisture damages, causes and repair measures*)(In Norwegian). SINTEF Building and Infrastructure. Oslo. Norway

Gullbrekken (2017) Ventilated wooden roofs: Influence of local weather conditions - measurements. *11th Nordic Symposium on Building Physics, NSB2017*, 11-14 June 2017, Trondheim, Norway

Hansen H.E, Kjerulf-Jensen P, Stampe O.B. (2013) *Varme og klimateknik Danvak Grundbog (Heat and climate technique Danvak)* (In Danish). 4. edition. Danvak. Denmark ISBN: 978-87-982652-0-7

Hofseth V. (2004) Studie av luftede takkonstruksjoner (Study of ventilated roof constructions) (In Norwegian). *NTNU.* Trondheim. Norway

Idelchik I.E. (1994) *Handbook of Hydraulic Resistance*: CRC Press. Florida. USA. ISBN:0-8493-9908-4

Kronvall J. (1980) Air flows in building components. PhD TVBH-1002. Lund University. Sweden

Roels S, Langmans J. (2016) Highly insulated pitched roofs resilient to air flow patterns: Guidelines based on a literature review. *Energy and Buildings* 120: 10-18.

Samuelson I. (1998) Hygrothermal Performance of Attics. *Journal of Thermal Envelope and Building Science* 22: 132-146.

Thiis T.K, Barfoed P, Delpech P, Gustavsen A, Hofseth V, Uvsløkk S, Dufresne de Virel M.(2007) Penetration of snow into roof constructions—Wind tunnel testing of

different eave cover designs. *Journal of Wind Engineering and Industrial Aerodynamics* 95: 1476-1485.
Tobiasson W, Buska J, Greatorex A. (1994) Ventilating attics to minimize icings at eaves. *Energy and Buildings* 21: 229-234.
Uvsløkk S. (1996) The Importance of Wind Barriers for Insulated Timber Frame Constructions. *Journal of Building Physics* 20: 40-62.